PERGAMON

International Journal of Heat and Mass Transfer 42 (1999) 2101–2110

International Journal of HEAT and MASS TRANSFER

Technical Note

Heat transfer characteristics of an axisymmetric jet impinging on the rib-roughened convex surface

Y.S. Chung[a], D.H. Lee[a,*], J.S. Lee[b]

[a] *School of Mechanical and Automotive Engineering, Inje University, 607 Obang-Dong, Kimhae, Kyungnam 621-749, Korea*
[b] *Department of Mechanical Engineering, Seoul National University, Silim-Dong, Kwanakgu, Seoul 151-742, Korea*

Received 16 January 1998; in final form 4 August 1998

Nomenclature

C specific heat of the Plexiglas (J/kg K)
C_P wall pressure coefficient ($=(p_w-p_\infty)/0.5\rho U_{ce}^2$)
d pipe nozzle diameter (m)
d_1 height of the rib (mm)
D outer diameter of the convex hemisphere (m)
h_c convective heat transfer coefficient (W/m^2 K)
h_r radiation heat transfer coefficient (W/m^2 K)
k thermal conductivity of the Plexiglas (W/m K)
L nozzle-to-surface distance (m)
Nu local Nusselt number
Nu_{ave} average Nusselt number over the curved surface
p pitch of the rib (mm)
p/d_1 dimensionless pitch-to-rib height
p_w wall pressure on the hemisphere surface (N/m^2)
p_∞ atmospheric pressure (N/m^2)
r streamwise distance from the stagnation point (m)
Re Reynolds number based on mean velocity and nozzle diameter ($=Ud/v$)
t time for the surface temperature difference (T_i-T_{LC}) to occur(s)
T_i initial temperature of the hemisphere (°C)
T_∞ ambient temperature (°C)
T_{LC} convex surface temperature measured by the liquid crystal (°C)
T_{ref} average surface temperature ($=0.5(T_i+T_{LC})$) (°C)
T^* dimensionless surface temperature.

Greek symbols

ε emissivity of the liquid crystal and black paint coated surface (measured by infrared radiation thermometer: Minolta/505S)
v kinematic viscosity of air (m^2/s)
ρ density of the Plexiglas (kg/m^3)
σ Stefan–Boltzmann constant ($=5.669\times10^{-8}$ W/m^2 K^4).

1. Introduction

Numerous studies of the impinging jet heat transfer and flow characteristics have been reported by Martin [1], Jambunathan et al. [2], Viskanta [3], Baughn and Shimizu [4], and Lee et al. [5]. Most of these studies have focused on the heat transfer enhancement in the stagnation point region. However, in order to increase an overall average heat transfer in the impinging surface, it is necessary to increase the heat transfer rate in the wall jet region where the heat transfer is relatively low compared to the stagnation point region. Miyake et al. [6], Cha et al. [7], and Hrycak [8] have investigated the heat transfer from the rib-roughened flat surface to impinging jets and presented the optimum conditions (i.e., rib height, shape, pitch, and nozzle-to-surface distance, etc.) for the maximum heat transfer to occur.

In the mean time, a literature search does not show any research results that deal with the impinging jet heat transfer from the rib-roughened curved surface. But, there are a few papers that studied the impinging jet heat transfer from the smooth curved surface. Hrycak [9] studied the heat transfer characteristics with round jets impinging on a concave surface. Gau and Chung [10] studied the effects of surface curvature on slot jet impingement heat transfer along the semi-cylindrical concave and convex surfaces. Yang et al. [11] investigated jet impingement cooling on the semi-cylindrical concave surface with round-edged and rectangular-edged nozzles. Lee et al. [12] studied the effects of the convex surface

* Corresponding author

0017–9310/99/$ - see front matter
PII: S0017-9310(98)00313-5

curvature on the local heat transfer by a fully developed round impinging jet.

The present study focuses on the heat transfer enhancement by the fully developed round jet impinging upon the rib-roughened convex surface. Heat transfer measurements were carried out using liquid crystal/transient technique for $Re = 23000$, $L/d = 6$–10, and three types of rib roughness elements (see Table 1).

2. Experimental apparatus and technique

A diagram of the test apparatus used in the experiment is shown in Fig. 1. The apparatus consists of a blower, a heat exchanger, an orifice flow meter, cast acrylic pipes with an inner diameter of $d = 2.15$ cm, and a rib-roughened convex surface. The development length-to-pipe diameter ratio of 58 results in a fully developed velocity profile of the jet flow at the nozzle exit.

Table 1
Specifications of the rib types

Types	Height (d_1) (mm)	Pitch (p) (mm)	p/d_1
A	2	12	6
B	2	22	11
C	2	32	16

Figure 2 shows a schematic diagram of the test model and shroud. The test model consists of a 3.5 mm thick and 38.1 cm diameter Plexiglas convex hemisphere. Circular ribs with a diameter of $d_1 = 2$ mm are mounted on the convex surface with 12, 22, and 32 mm gaps between the ribs (see Table 1). In order to make a strong contact between the surface and the ribs, a liquid type super glue is used. An air brush is used to apply first the micro-encapsulated thermochromic liquid crystal (HALLCREST 'R29C4W') and then black backing paint on the test model surface. The test model is placed in a specially designed constant temperature air oven, made of 6 cm thick Styrofoam insulation, which is in the form of shroud. Now the test model is heated in the oven for 4–5 h during which the temperature of the test model becomes uniform within $\pm 0.2^{\circ}$C. When the test model reaches a desired temperature (about 8°C above the temperature in which the liquid crystal color begins to occur), the shroud is suddenly removed and the test model is exposed to the impinging jet flow. The fast removal of the shroud initiates the transient process. As the test model is cooled down, the color change of the liquid crystal occurs at a given time. A digital color image processing system is used to quantitatively determine the temperature corresponding to a particular color of liquid crystal.

The principle of the liquid crystal/transient technique is to calculate the local heat transfer coefficient using a temperature difference between surface and ambient fluid, and an elapsed time for this difference to occur. A one-dimensional heat conduction approximation is used since the surface temperature response is limited to a

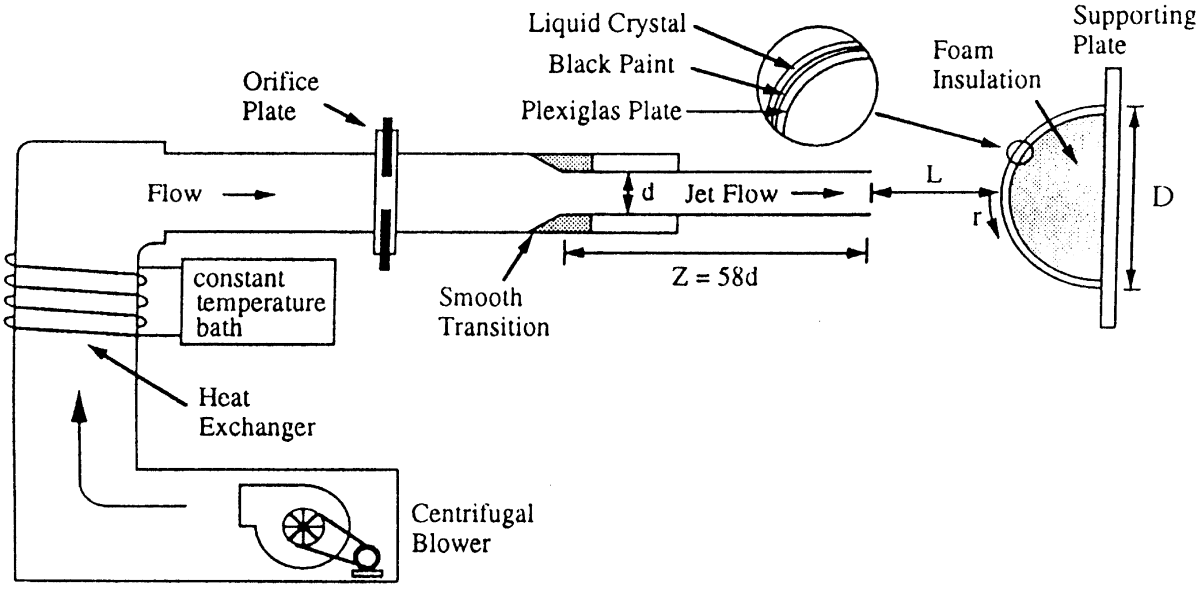

Fig. 1. Schematic diagram of the test apparatus for the jet impingement on the rib-roughened convex surface.

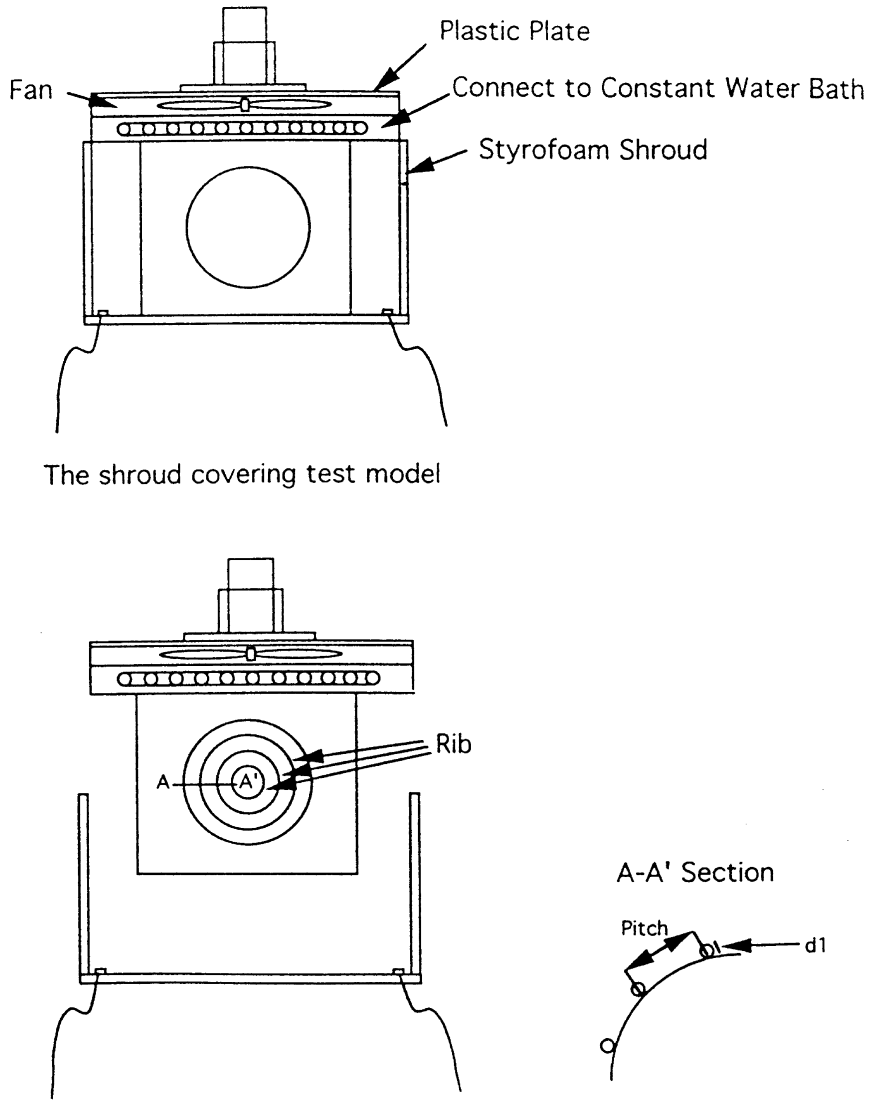

Fig. 2. Schematic diagram of the test model.

thin layer near the surface and lateral conduction can be shown to be small (Baughn and Yan [13]). Therefore, one-dimensional conduction into a semi-infinite medium with a convective boundary condition is assumed and it has the following solution

$$T^* = \frac{T_{LC} - T_\infty}{T_i - T_\infty} = e^{\gamma^2}\mathrm{erfc}(\gamma) \tag{1}$$

where T_{LC} is the surface temperature determined by liquid crystal, T_∞ is the ambient fluid temperature, and T_i is the initial surface temperature. In eqn (1)

$$\gamma = \frac{(h_c + h_r)\sqrt{t}}{\sqrt{\rho Ck}} \tag{2}$$

Now, the convective heat transfer coefficient h_c is calculated as

$$h_c = \frac{\gamma\sqrt{\rho Ck}}{\sqrt{t}} - h_r \tag{3}$$

where t represents the time for the surface temperature difference $(T_i - T_{LC})$ to occur, h_r is the radiation heat

transfer coefficient ($=\varepsilon\sigma(T_{ref}+T_\infty)\ (T_{ref}^2+T_\infty^2)$), ε is the emissivity of the liquid crystal/black paint coated surface, and T_{ref} is the average surface temperature ($=0.5(T_i+T_{LC})$).

The uncertainty analysis has been carried out using the method suggested by Kline and McKlintock [14]. It is shown in Table 2 that the overall uncertainty in the Nusselt number for $L/d=10$, $r/d=0.7$, and $p/d_1=11$ at $Re=23000$ is 6.95%. It should be noted that this uncertainty represents the maximum uncertainty in the Nusselt number under the given conditions. The uncertainty in the property of Plexiglas is the largest contribution to the overall uncertainty.

3. Results and discussion

Figure 3 shows the flow pattern models, suggested by Webb et al. [15], on the flat surface with repeated-rib roughness for the dimensionless pitch-to-rib height of $p/d_1=6$ and $p/d_1\geqslant 10$. For $p/d_1=6$, the free flow passing over the rib reattaches on the floor, and for $p/d_1\geqslant 10$, the boundary layer begins to grow after the flow reattachment on the floor. Webb et al. [15] also showed that the flow separation occurs on top of the rib element and the flow reattaches at $p/d_1\approx 6$–8 depending on the shape of the rib roughness.

The profiles of the wall pressure coefficient along the smooth and rib-roughened surfaces (rib type C) for $L/d=6$ and 10 at $Re=23000$ are shown in Fig. 4. For the smooth surface case, C_p gradually decreases from its maximum value at the stagnation point to zero at $r/d\cong 1.5$ to slight negative value in the region beyond $r/d=1.5$, and the pressure recovers to positive value at $r/d\cong 5.5$. But, for the rib-roughened surface case, the pressure suddenly increases when the flow collides on the upstream of the rib. As the fluid flows over the rib, the flow separation occurs on top of the rib, which in turn creates a low pressure region downstream of the rib. However, although we can see a tiny but finite change in pressure coefficient around $r/d\cong 6.0$ for the rib-roughened surface, the pressure coefficient is hardly changed in the region beyond $r/d\cong 6.0$. This may be attributed to a drastic decrease of the flow momentum in the region far away from the stagnation point when the fluid flows over the curved surface. This behavior is in good agreement with the heat transfer results to be introduced shortly.

Table 2
Nusselt number uncertainty analysis

X_i	Value	δX_i	$\left(\frac{\delta X_i}{Nu}\frac{\partial Nu}{\partial X_i}\right)\times 100$ (%)
T_∞	21.45 (°C)	0.15	1.42
T_{LC}	29.06 (°C)	0.25	4.45
T_i	37.7 (°C)	0.15	1.25
t	2.7 (s)	0.03	0.6
$\sqrt{\rho Ck}$	335	16.75	4.95
ε	0.9	0.05	0.1
d	0.0215 (m)	5.0×10^{-5}	0.2

Total Nu uncertainty: $\delta Nu/Nu=6.95\%$.

The local Nusselt number distributions along the convex surfaces with three rib types (A, B, C) are presented in Figs 5–7 for $d_1=2$ mm and $p/d_1=6$, 11, 16 at $L/d=6$ and 10. Figure 5 shows the local Nusselt number distributions with rib type A (i.e., $p/d=6$). From the stagnation point to the first rib position ($r/d\cong 0.56$), the Nusselt numbers on the rib-roughened surface are slightly lower than those on the smooth surface. Apparently, the rib obstructs the flow and the momentum of the flow is reduced, which in turn reduces the heat transfer rate. This phenomenon is more marked for $L/d=10$ than for $L/d=6$. However, after the first rib position, due to an increase of the turbulent intensity and active mixing of the flow caused by the flow separation, the Nusselt numbers on the rib-roughened surface are higher than those on the smooth surface. This trend appears to continue until $r/d\cong 5.0$.

Figure 6 shows the Nusselt number distributions with rib type B (i.e., $p/d_1=11$). Near the stagnation point, the Nusselt number distributions for both smooth surface and rib-roughened surface are similar. Unlike Fig. 5, the Nusselt number sharply decreases and increases just before and after the first rib position. In the case of $p/d_1\geqslant 10$, the heat transfer rate increases due to both the flow separation and the reattachment, as shown in Fig. 3. Consequently, the rate of heat transfer enhancement with rib type B is higher than with rib type A. After the flow reattachment, the boundary layer begins to grow and as a result, the Nusselt number sharply decreases. When the flow approaches the second rib position, the flow separation, reattachment, and boundary layer growth are repeated and the Nusselt number either increases or decreases accordingly. This can be seen up to the third rib position ($r/d\cong 3.0$). It should also be noted that the rate of the heat transfer enhancement by the first rib is more than 4 times as high as that by the second rib.

Figure 7 shows the Nusselt number distributions with rib type C (i.e., $p/b_1=16$). In the region corresponding to $0\leqslant r/d<1.0$, because of the large gap between ribs, the Nusselt number distributions are similar to those on the smooth surface. In the region of $r/d\geqslant 1.0$, due to a momentum loss by the increasing pressure just before the first rib position, the Nusselt number on the rib-roughened surface tends to be lower than that on the smooth surface and attains a minimum value at $r/d\cong 1.3$. Further downstream, the Nusselt number sharply increases and attains a secondary peak (approximately 93 and 96% of the stagnation point Nusselt number for $L/d=6$ and $L/d=10$, respectively) at $r/d\cong 1.7$. As the

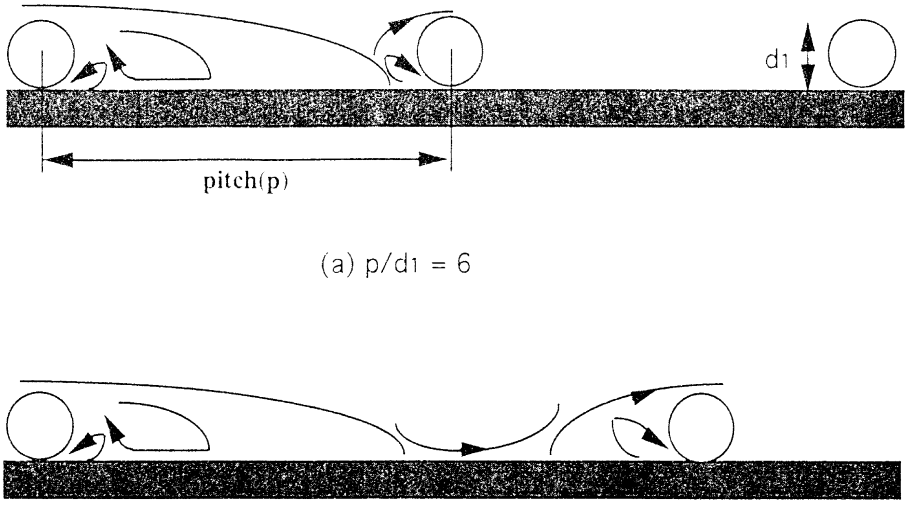

Fig. 3. A model of flow pattern on a rib-roughened surface.

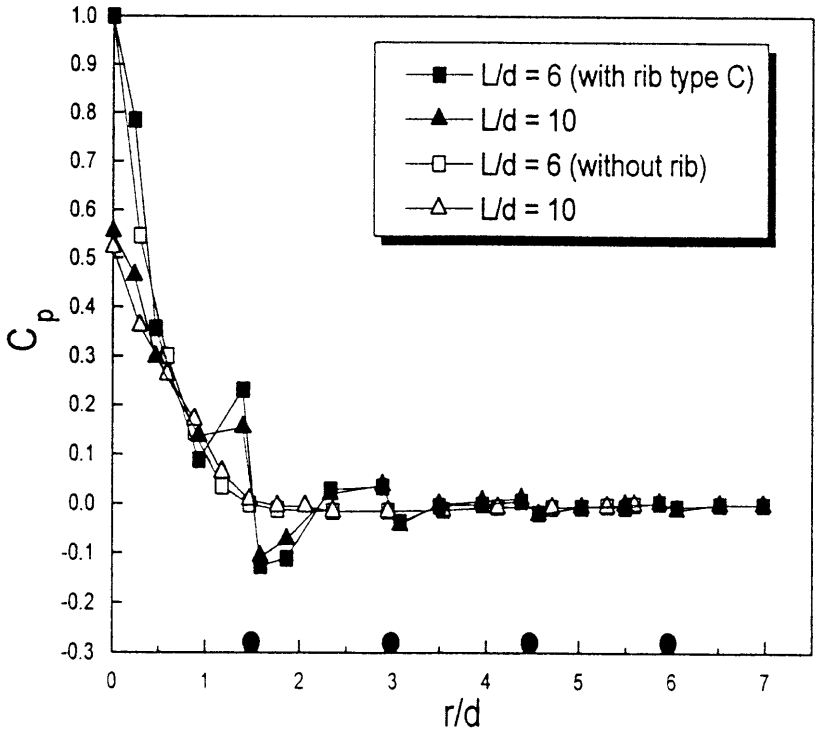

Fig. 4. Profiles of the wall pressure coefficient along the convex surface without rib and with rib type C at $Re = 23000$.

boundary layer grows, the Nusselt number sharply decreases from its secondary maximum value. Especially for $L/d = 6$, it drops down below the value on the smooth surface. On the other hand, the Nusselt number before and after the second rib position decreases and increases, respectively, due to similar flow phenomena previously

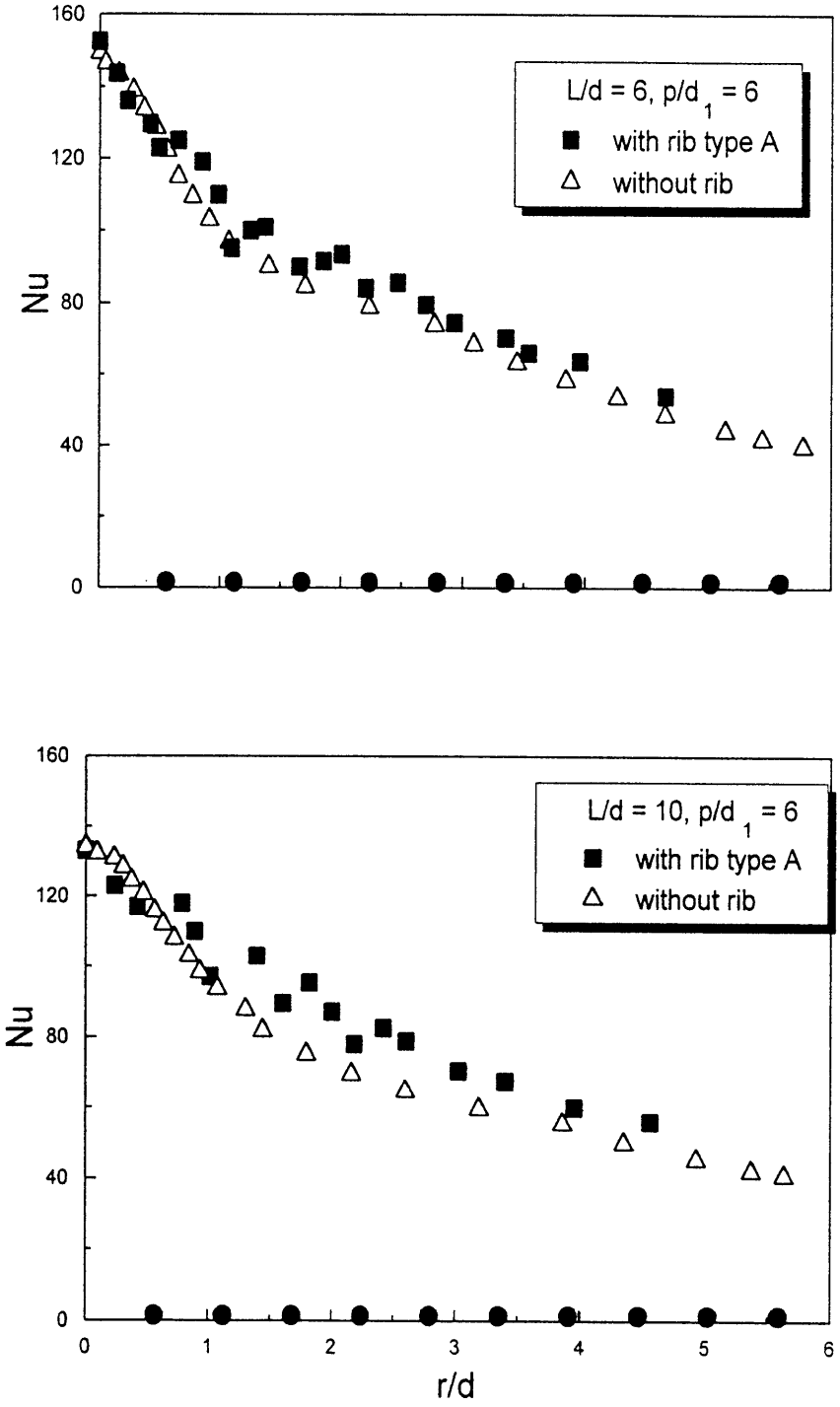

Fig. 5. Comparison between the Nusselt number on the convex surface without rib and with rib type A for $p/d_1 = 6$.

described and its variation is less than 20% of that which occurred at the first rib. It turns out that the third rib ($r/d \cong 5.0$) does not affect the heat transfer rate any more.

All of the heat transfer behaviors described above are in excellent agreement with the profiles of the wall pressure coefficient shown in Fig. 4.

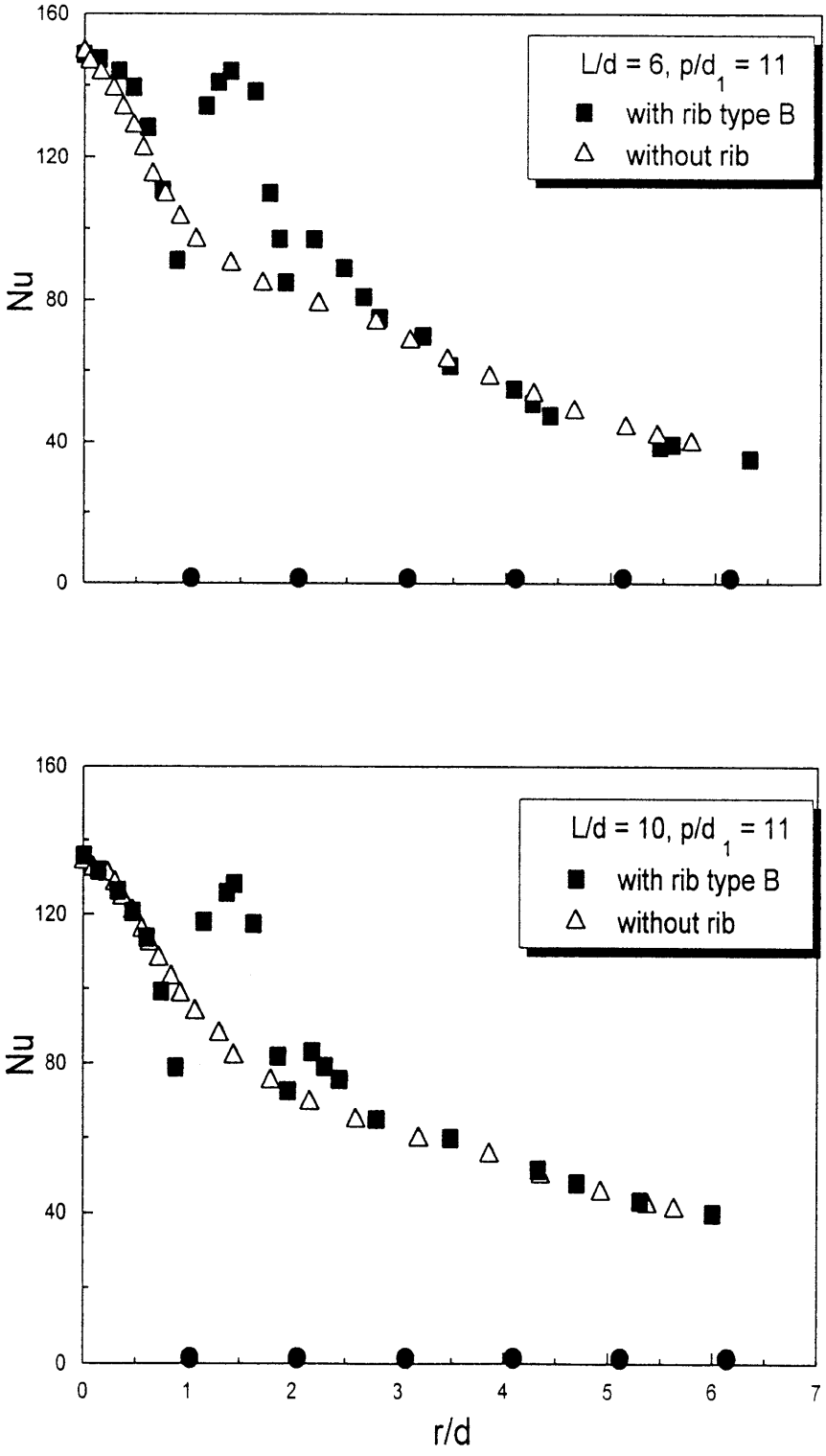

Fig. 6. Comparison between the Nusselt number on the convex surface without rib and with rib type B for $p/d_1 = 11$.

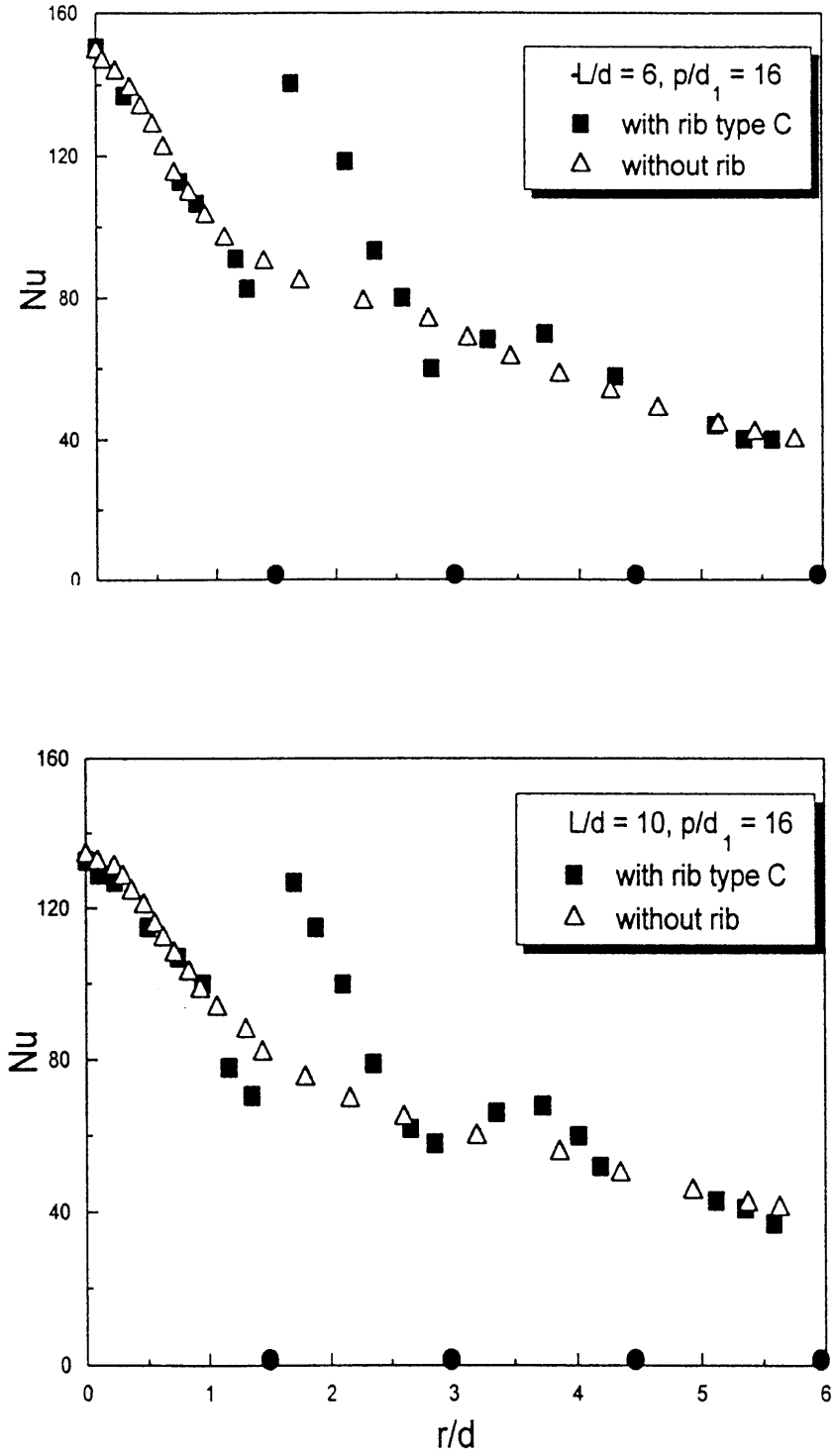

Fig. 7. Comparison between the Nusselt number on the convex surface without rib and with rib type C for $p/d_1 = 16$.

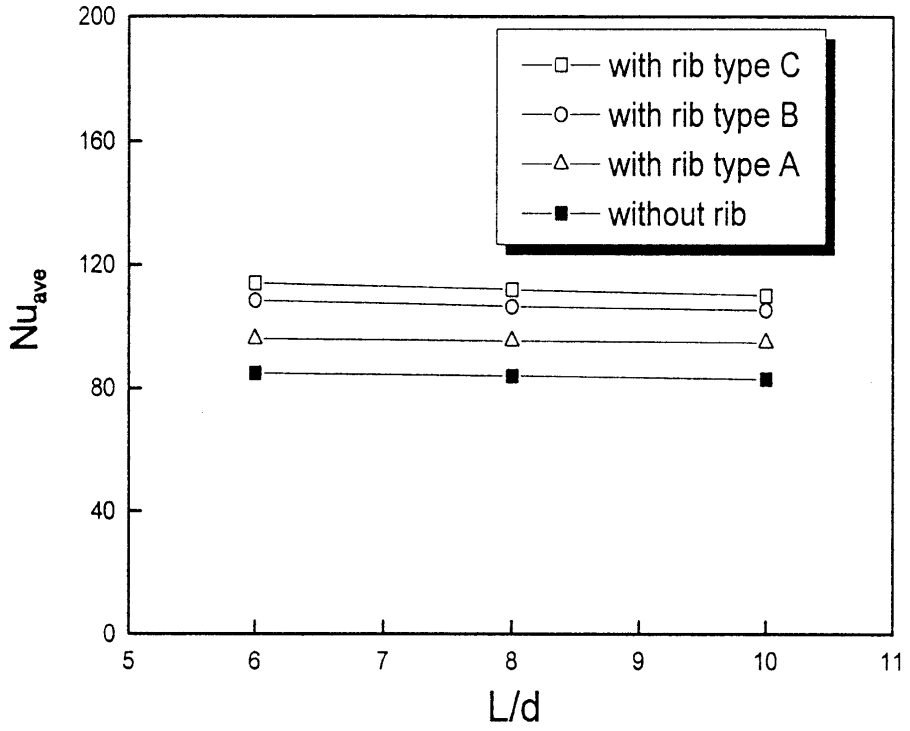

Fig. 8. Comparison between the average Nusselt number on the convex surface without rib and with rib types of A, B and C.

The average Nusselt number distributions on the smooth and rib-roughened surfaces for $L/d = 6, 8, 10$ are shown in Fig. 8. It follows that compared with the smooth surface, the average Nusselt number on the rib-roughened surface increases by maximum 14, 27, and 34% for rib types A, B, and C, respectively. This is attributed to an increase of the turbulent intensity caused by the flow separation, recirculation, and reattachment. On the other hand, rib types B and C produce a higher average heat transfer rate than rib type A. It is due to a different heat transfer enhancement mechanism, i.e., by the flow separation and recirculation for $p/d_1 \geqslant 10$ and by the flow separation only for $p/d_1 \leqslant 6$. This result is in a good agreement with results of Webb et al. [15].

4. Conclusions

The experimental study has been carried out to investigate the flow and heat transfer characteristics by jets impinging upon the rib-roughened convex surface. For $p/d_1 = 6$, near the stagnation point, the Nusselt number distributions for both smooth and rib-roughened surfaces are similar. However, after the first rib position, due to an increase of the turbulent intensity and active mixing of the flow caused by the flow separation, the Nusselt numbers on the rib-roughened surface are higher than those on the smooth surface. And, in the case of $p/d_1 \geqslant 10$, the heat transfer rate increases due to both the flow separation and the reattachment.

The average Nusselt number on the rib-roughened surface increases by maximum 14, 27, and 34% for three rib types A, B, and C, respectively, compared with that on the smooth surface. This is attributed to an increase of the turbulent intensity caused by the flow separation, reattachment and recirculation. On the other hand, rib types B and C produce a higher heat transfer rate than rib type A. It is due to a different heat transfer enhancement mechanism, i.e., by the flow separation and recirculation for $p/d_1 \geqslant 10$ and by the flow separation only for $p/d_1 \leqslant 6$. Beyond the region corresponding to $r/d \cong 4.0$–6.0, the rib roughness does not affect the heat transfer any more.

References

[1] H. Martin, Heat and mass transfer between impinging gas jets and solid surfaces, Advances in Heat Transfer 13 (1997) 1–60.
[2] K. Jambunathan, E. Lai, M.A. Moss, B.L. Button, A review of heat transfer data for single circular jet impingement, Int. Journal of Heat and Fluid Flow 13 (1992) 106–115.
[3] R. Viskanta, Heat transfer to impinging isothermal gas

and flame jets, Experimental Thermal and Fluid Science 6 (1993) 111–134.
[4] J.W. Baughn, S.S. Shimizu, Heat transfer measurements from a surface with a uniform heat flux and a fully developed impinging jet, ASME Journal of Heat Transfer 111 (1989) 1096–1098.
[5] D.H. Lee, R. Grief, S.J. Lee, J.H. Lee, Heat transfer from a flat plat to a fully developed axisymmetric impinging jet, ASME. Journal of Heat Transfer 117 (1995) 772–776.
[6] G. Miyake, M. Hirata, N. Kasagi, Heat transfer characteristics of an axisymmetric jet impinging on a wall with concentric roughness elements, Experimental Heat Transfer 7 (1994) 121–141.
[7] J.Y. Cha, N. Kasagi, M. Hirata, Structure of a two-dimensional jet impinging on the wall with large-scale transverse repeated roughness (in Japanese), Journal of Flow Visualization Soc. Japan 4 (1984) 223–228.
[8] P. Hrycak, Heat transfer from impinging jets to flat plate with conical and ring protuberances. Int. Journal of Heat and Mass Transfer 27 (1984) 2145–2154.
[9] P. Hrycak, Heat transfer and flow characteristics of jets impinging on a concave hemispherical plate, Proceedings of 7th International Heat Transfer Conference 3 (1982) 357–362.
[10] C. Gau, C.M. Chung, Surface curvature effect on slot-air jet impingement cooling flow and heat transfer process, ASME Journal of Heat Transfer 113 (1991) 858–864.
[11] G.Y. Yang, M.S. Choi, J.S. Lee, An experimental study of jet impinging cooling on the semi-circular concave surface, Trans. Korea. Soc. Mech Eng. 19 (1995) 1083–1094.
[12] D.H. Lee, Y.S. Chung, D.S. Kim, Turbulent flow and heat transfer measurements on a curved surface with a fully developed round impinging jet, Int. Journal of Heat and Fluid Flow 18 (1997) 160–169.
[13] J.W. Baughn, X. Yan, Local heat transfer measurements in square ducts with transverse ribs, HTD-202 (1992) 1–7.
[14] S.J. Kline, F.A. McKlintock, Describing uncertainties in single sample experiments, Mechanical Engineering 75 (1953) 3–8.
[15] R.L. Webb, E.R.G. Eckert, R.J. Goldstein, Heat transfer and friction in tubes with repeated-rib roughness, Int. Journal of Heat and Mass Transfer 14 (1971) 601–617.